Air-sea Interaction under Hurricane Wind Conditions

Yuliya Troitskaya, Daniil Sergeev,
Alexander Kandaurov and Vasilii Kazakov
Institute of Applied Physics
Russia

1. Introduction

One of the main characteristics appearing in the models of forecasting wind over the sea is the roughness of the sea surface determined by the parameters of the wind waves, quantitatively parameterised by the sea surface drag coefficient C_D. To define it we introduce the turbulent shear stress or turbulent momentum flux far from the sea surface

$$\tau_{turb}(z) = \rho_a u_*^2 \, , \tag{1}$$

where ρ_a is the air density, u_* is the wind friction velocity. Wind is the turbulent boundary layer with the logarithmic mean velocity profile:

$$U(z) = \frac{u_*}{\kappa} \ln \frac{z}{z_0} \, , \tag{2}$$

Similar to the resistance law of the wall turbulent flow the sea surface drag coefficient is introduced as follows:

$$C_D = \frac{\tau_{turb}}{\rho_a U_{10}^2} = \frac{u_*^2}{U_{10}^2} \, , \tag{3}$$

where U_{10} -the wind velocity at a standard meteorological height H_{10}=10 m. which relate this coefficient to U_{10} are obtained either by generalizing empirical data (Garratt, 1977; Large & Pond, 1981, Taylor & Yelland, 2002; Fairall et al., 2003) or by numerical models (see, for example, Janssen, 1989; Janssen, 1991, Makin et.al, 1994; Hara & Belcher, 2004). Numerous field measurements give increasing dependencies of C_D on wind speed, which relates to increasing of wave heights with the wind.

The aerodynamic drag coefficient of the sea surface is a critical parameter in the theory of tropical hurricanes (Emanuel, 1995). To illustrate it we consider here the ideas of theory of energy balance in a tropical cyclone suggested by (Emanuel, 1986; Emanuel, 1995, Emanuel, 2003). According to this theory the mature tropical cyclone may be idealized as a steady, axisymmetric flow whose energy cycle is very similar to that of an ideal Carnot engine,

where the hot reservoir is the ocean with the temperature T_S and the cold reservoir is .the troposphere with the temperature T_0. The details of construction and operation of this heat engine are presented in (Emanuel, 1986; Emanuel, 1995, Emanuel, 2003), but one of the most important characteristics of a tropical cyclone, the maximum surface wind velocity, which determines its category, can be estimated without details from the Carnot theorem.

According to the Carnot theorem, the maximum efficiency of the ideal heat engine is determined by the absolute temperatures of the hot and cold reservoirs:

$$\eta = \frac{W}{Q_s} = \frac{T_s - T_0}{T_0} \, , \tag{4}$$

where Q_s is the heat energy entering the system from the hot reservoir and W is the mechanical work done by the system. Heat energy support of the tropical cyclone comes from the ocean (heat flux from the sea surface) and mechanical energy dissipated in the marine turbulent boundary layer (Emanuel, 2003), the heat energy entering the system is the surface integral of the heat flux from the sea F_q and mechanical energy dissipation rate F_p:

$$Q_s = \int \left(F_q + F_p \right) ds \tag{5}$$

Mechanical work done by the system compensates mechanical energy dissipation, then

$$W = \int F_p ds \tag{6}$$

The heat flux from the sea and the mechanical energy dissipation rate are determined by the bulk formula:

$$F_q = C_k \rho \left| \vec{V} \right| \left(k_0 - k \right) \tag{7}$$

here k_0, k are enthalpy at the sea level and in marine atmospheric boundary layer.

$$F_p = C_D \rho \left| \vec{V} \right|^3 \tag{8}$$

In (7)-(8) C_k is heat exchange coefficient (or the Stanton number), C_D is surface drag coefficient, defined by equation (3).

Taking into account the Carnot theorem (4) and estimating integrals (5) and (6) yields estimate for the maximum surface wind velocity in a tropical cyclone as a function of ratio C_D/C_k.:

$$\left| \vec{V} \right|_{max} = \sqrt{\frac{C_k}{C_D} \frac{T_s - T_0}{T_0} \left(k - k_0 \right)} \tag{9}$$

Conventional bulk formulas, derived by generalizing experimental data (Garratt, 1977; Large & Pond, 1981, Taylor & Yelland, 2002; Fairall et al., 2003) obtained at wind velocities less than 30 m/s, overestimate the drag coefficient of the sea surface under hurricane winds. The estimates presented in (Emanuel, 1995) indicate that energy dissipation due to friction

proves too high to explain the observed velocity of a hurricane wind for realistic sources of energy.

The problem of explaining high wind velocities during hurricanes can be resolved if the drag coefficient of the sea surface does not increase with increasing wind velocity. To explain high quantities of wind speeds observed in tropical cyclones Emanuel, 1995 suggested that the drag coefficient flattens and even decreases at high wind speed in contradiction with intuition, since, it follows then, that sea surface should be effectively smoothed under the hurricane conditions. However, in the late 90-th these dependencies were observed experimentally in the field and laboratory conditions (Powell et al, 2003).

2. Observations of the sea surface drag reduction

The effect of sea surface drag reduction under hurricane wind was discovered by (Powell et al, 2003) in their experiments on measurements of the wind velocity profiling in the marine atmospheric boundary layer associated with tropical cyclones by 331 Global Positioning System sondes dropped in 15 storms. The wind friction velocity u* can be easily retrieved from equation (2) and sea surface drag can be calculated from its definition (3). Analysis of these measurements in (Powell et al, 2003) showed that that the drag coefficient of the sea surface is much less than the extrapolation of data measured at "usual winds" and even decreases if the wind velocity exceeds 30–35 m/s (see fig.1a). More precisely, according to (Powell, 2007) surface drag depends significantly on the sector of the tropical cyclone, where it is measured.

The similar dependencies of the surface drag coefficient on the wind speed were retrieved from the measurements of the ocean currents driven by the tropical cyclone Andrew (Jarosz et al., 2007). As it was reported in (Jarosz et al., 2007) on 15 September 2004, the centre of Hurricane Ivan passed directly over current and wave/tide gauge moorings on the outer continental shelf in the north-eastern Gulf of Mexico. Analysis of the along-shelf momentum balance in the water column, when the current structure was frictionally dominated was made within the following equation:

$$\frac{\partial U}{\partial t} - fV = \frac{\tau_{sx}}{\rho H} - \frac{rU}{H} \tag{10}$$

(where U and V are depth-integrated along- and cross-shelf current velocity components, f is the Coriolis parameter, $\boldsymbol{\rho}$ is the water density, τ_{sx} is the along-shelf wind stress component, H is the water depth, and r is the constant resistance coefficient at the sea floor). Equation (10) enables one to retrieve the wind stress τ_{sx} and estimate the sea surface grad coefficient by of the equation (3) using independently measured wind velocity. The results produced from evaluation of this procedure presented in (Jarosz et al., 2007) show a decreasing trend of C_D for wind speeds greater than 32 m s^{-1} (see fig.1b).

So field measurements of the wind stress both from the atmospheric and ocean sides of the air-sea interface show that the sea surface drag coefficient is significantly reduced at hurricane wind speeds in comparison with the extrapolation of the experimental data obtained at "normal" wind speeds and even decreases for U_{10} exceeding 35 m/s.

The similar effect was observed in laboratory experiments performed at the Air-Sea Interaction Facility at the University of Miami (Donelan et al., 2004). In that experiment the
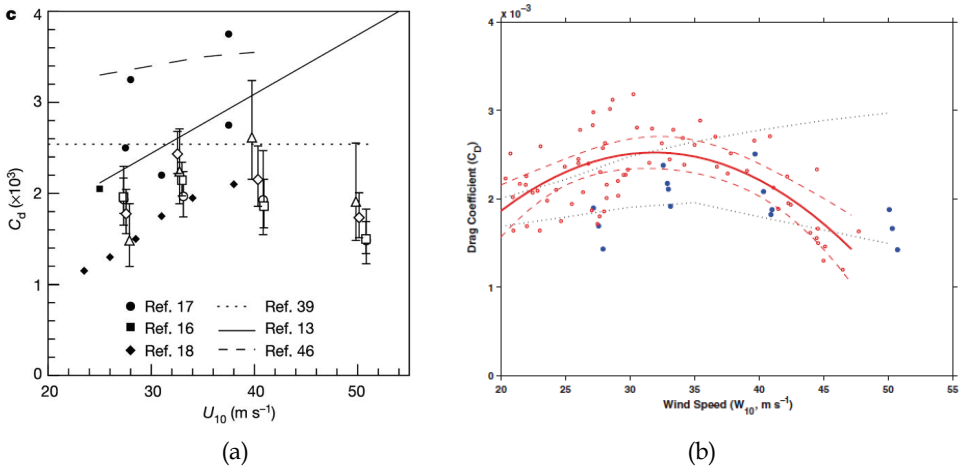
(a)   (b)

Fig. 1. Sea surface drag coefficient via 10-m wind speed: (a) – from Powel et.al, 2003, (b) – from science, 2007.

aerodynamic resistance of the water surface was measured by three different methods: using the profile method (in which the vertical gradient of mean horizontal velocity is related to the surface stress), the Reynolds stress method, and the momentum budget method based on analysis of a momentum budget of water column sections of the tank (Donelan et al., 2004). In comparison with two others, the latter method is insensitive to droplets suspended in the airflow at high wind speeds. The wind speed was measured at 30 cm height in the tank and extrapolated to the standard meteorological height of 10 m using the well-established logarithmic dependence on height (Donelan et al., 2004). All methods were in excellent agreement, and the momentum budget method enabled Donelan et al 2004 to measure the wind stress and aerodynamic resistance coefficient of the water surface up to equivalent 10-m wind speeds about 60 m/s. Figure 2 from (Donelan et al., 2004)
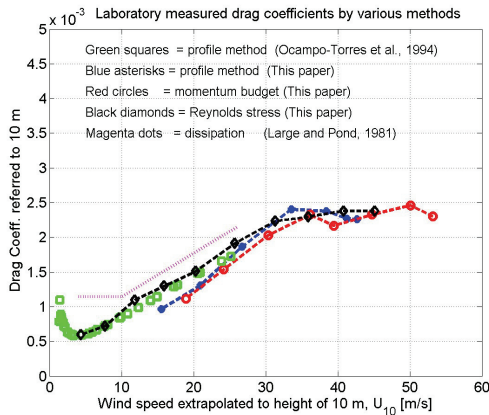

Fig. 2. Laboratory measurements of the neutral stability drag coefficient (reproduced from Donelan etal, 2004)

demonstrates a remarkable levelling of the drag coefficient for the 10-m wind speed exceeding 33 m/s. The difference between C_D dependencies on the wind speed in field and laboratory experiments is discussed in (Donelan et al., 2004). Possibly it is due to strong inhomogeneity and non-stationarity of the wind in the hurricane eye walls, where the constant stress concept derives from the boundary layer Reynolds equations is not confirmed.

So it can be concluded both from field and laboratory data, that the growth of the aerodynamic roughness of the water surface with wind speed is significantly reduced at extremely high winds in spite of increasing of surface wave heights. Several theoretical models were suggested for explanation of this empirical fact.

3. Possible mechanisms of the sea surface drag reduction at extreme wind speeds

Among a number of possible theoretical mechanisms suggested for explanation of the effect of the sea surface drag reduction at hurricane winds two groups of the models can be specified. First, (Kudryavtsev & Makin, 2007) and (Kukulka et al., 2007) explain the sea surface drag reduction by peculiarities of the airflow over breaking waves, which determine the form drag of the sea surface. For example, in (Donelan et al., 2004), the stabilization of the drag coefficient during hurricane winds is qualitatively explained by a change in the shape of the surface elevation in dominant waves at wind velocities above 35 m/s, which is accompanied by the occurrence of a steep leading front. In this case, occurrence of flow separation from the crests of the waves is assumed. This assumption is based on the laboratory experiments by (Reul et al., 1999), where airflow separation was observed at the crests of breaking waves by the PIV method. According to hypothesis by Donelan et al, 2004, existence of the airflow trapped in the separation zone skips the portions of the water surface in the troughs of the waves and thus, in conditions of continuous breaking of the largest waves the aerodynamic roughness of the surface is limited. Besides, generation of small-scale roughness within the separation zone is reduced due to sheltering, which can also reduce the surface resistance. This effect is expected to be dominant for the case of young sea (or in laboratory conditions as in (Donelan et al., 2004), when wave breaking events are not rare even for energy containing part of the surface wave spectrum.

Another approach more appropriate for the conditions of developed sea exploits the effect of sea drops and sprays on the wind-wave momentum exchange (Andreas & Emanuel, 2001, Andreas, 2004, Makin, 2005, Kudryavtsev, 2006). (Andreas & Emanuel, 2001) and (Andreas, 2004) estimated the momentum exchange of sea drops and air-flow, while (Makin, 2005) and (Kudryavtsev, 2006) focused on the effect of the sea drops on stratification of the air-sea boundary layer similar to the model of turbulent boundary layer with the suspended particles by (Barenblatt & Golitsyn 1974). Suspended heavy particles (drops) in the marine turbulent boundary layer create stable stratification suppressing the turbulence, and then decreasing the effective viscosity of the turbulent flow and the aerodynamic resistance. In the same time, there is another effect of sea drops, the particles injected from the water surface should be accelerated, and then they consume some momentum flux from the airflow, increasing the surface drag in the turbulent boundary layer.

In the paper by (Troitskaya & Rybushkina, 2008) the sea surface drag reduction at hurricane wind speed is explained by reducing efficiency of wind-wave momentum exchange at hurricane conditions due to sheltering, but sheltering without separation. This assumption

is motivated by reports of eye-witnesses of strong ocean storms, who confirmed that the sea at hurricane wind is unexpectedly smooth and wave breaking is a relatively rare event (see references in (Andreas, 2004). Relatively smooth water surface presents at the video-films taken on board of the research vessel ``Viktor Buinitsky'', when it passes a polar lo in the Laptev sea and the Kara sea in October 2007 (cruise within the project NABOS - Dr.Irina Repina private communication). These visual observations are also confirmed by the instrumental measurements by (Donnely et al., 1999),, who observed saturation of the C-band and Ku-band normalized radar cross-section (NRCS) for wind speed above 25-30 m/s. Similar reduction of NRCS was observed in the laboratory tank experiments by (Donelan et al., 2004). Microwave power scattered from the water surface is formed by i) the Bragg scattering at short waves and ii) by reflection from wave breakers, i.e. the NRCS reduction supports evidence of smoothing of the sea surface by reducing both short wave roughness and wave breaking events. Mechanisms of unusual smoothness of the sea surface are unknown. (Andreas, 2004) suggested two possible explanations of this effect. One supposes the effect of bubbles on surface tension. Another possible explanation exploits the effect of spume drops torn from the wave crests by wind and then falling back as a kind of strong rain, which causes effective damping of surface waves according to a number of experiments (see ex. (Tsimplis, & Thorpe, 1975).

In spite of a number of theoretical hypotheses the problem of explanation of the effect of surface drag reduction at hurricane winds is not solved mostly due to the lack of experimental data.

4. Laboratory modelling of the air-sea interaction under hurricane wind

In this section we describe the results of new laboratory experiments devoted to modelling of air-sea interaction at extremely strong winds.

4.1 Experimental setup and instruments

The experiments were performed in the wind-wave flume built in the Large Thermostratified Tank of the Institute of Applied Physics. The centrifugal fan equipped with an electronic frequency converter to control the discharge rate of airflow produces the airflow in the flume with the straight part 10 m. The operating cross section of the airflow is 40*40 cm², whereas the sidewalls are submerged at a depth of 30 cm. Wave damping beach made of a fine mesh is placed at the airflow outlet at the end of the flume.

Aerodynamic resistance of the water surface was measured by the profile method at a distance of 7 m from the outlet. Wind velocity profiles were measured by the L-shaped Pitot tube intended for measuring flow velocities of up to 20 m/s (the axis velocity in the flume 25 m/s approximately corresponds to U_{10}=50-60 m/s). Simultaneously with the airflow velocity measurements, the 3-channel string wave gauge measured waves at the water surface. The experiment was accompanied by video shooting of the top view of the water surface.

4.2 Peculiarities of the profile method for measuring surface drag coefficient in aerodynamic tunnels

The classical profiling method of measuring surface drag coefficient is based on the property of steady wall turbulent boundary layer to conserve tangential turbulent stress u_*^2, then the average flow velocity is logarithmic and the wind friction velocity u_* can be easily

determined from (2), if the velocity profile is measured. However developing turbulent boundary layers are typical for the aerodynamic tubes and wind flumes, then three sub-layers at different distances from the water can be specified: viscous sub-layer, layer of constant fluxes and "wake" part (see fig.3a). The viscous sub-layer, where viscous effects are essential, exists over the hydrodynamically smooth surfaces at the distances less than $20 \div 30$ ν/u_* (ν is the kinematic viscosity), for moderate winds it is about 1 millimetre. The "wake" part is the outer layer of the turbulent boundary layer, where the boundary layer flow transits to the outer flow in the tube. Its thickness δ increases linearly from the outlet of the flume. The layer of constant fluxes is extended from the upper boundary of the viscous sub-layer to approximately 0.15δ. Only in the layer of constant fluxes the flow velocity profile is logarithmic and can be extrapolated to the standard meteorological height H_{10}. Typically in wind flumes the constant layer thickness is less than 10 cm. Measuring of wind velocity profiles at the distance less than 10 cm from the wavy water surface at strong winds is a difficult problem mainly due to the effect of sprays blown from the wave crests. Fortunately, parameters of the layer of the constant fluxes can be retrieved from the measurements in the "wake" part of the turbulent boundary layer, because the velocity profile in the developing turbulent boundary layer is the self-similar "law of wake" (see Hinze, 1959). The self-similar variables for the velocity profile and vertical coordinates are z/δ and $(U_{max}-U(z))/u_*$, where U_{max} is the maximum velocity in the turbulent boundary layer. The self-similar velocity profile can be approximated by the following simple equations (see Hinze, 1959):

- in the layer of constant fluxes

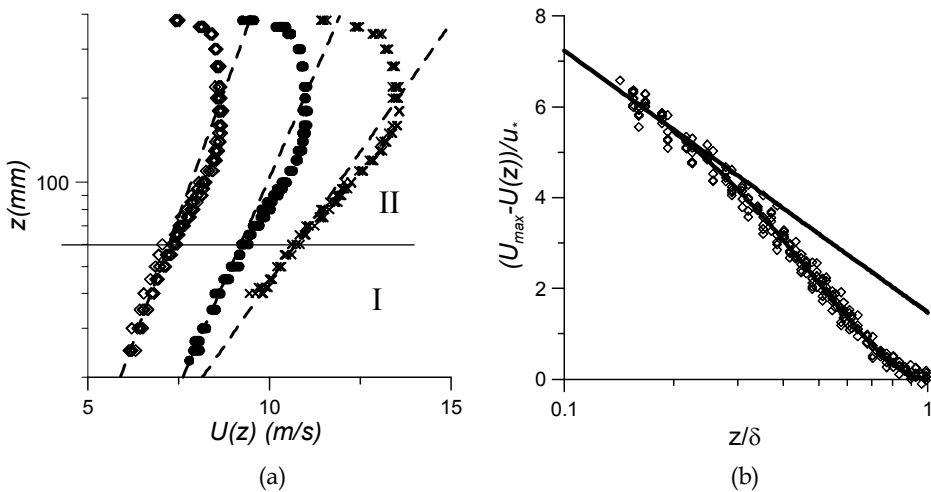$$U_{\max} - U(z) = u_* \left(-2.5\ln(z/\delta) + \alpha\right), \tag{11}$$

Fig. 3. Airflow velocity profiles in the aerodynamic flume over the waves for different airflow velocities (a); dashed curves are logarithmic approximations in the layer of constant fluxes. I – the layer of constant fluxes, II – the "wake" part. Air-flow velocity profiles measured at different wind speeds over waves in self-similar variables (b).

in the "wake" part

$$U_{\max} - U(z) = \beta u_* (1 - z/\delta)^2 \, . \tag{12}$$

Collapse of all the experimental points in one curve in self-similar variables occurred in our experiments (see fig.3b). The parameters in equations (11) (12) were obtained by the best fitting of the experimental data: $\alpha=1.5$, $\beta=8.5$.

The parameters of the logarithmic boundary layer can be retrieved from the measurements in the wake part of the turbulent boundary layer, first, retrieving parameters of turbulent boundary layer (U_{max} and δ) by fitting experimental data by equation (12) and then calculating parameters of the logarithmic boundary layer by the following expressions:

$$U(z) = 2.5u_* \ln(z/z_0) \, , \tag{13}$$

where

$$z_0 = \delta \exp(-\kappa U_{\max}/u_* + \alpha\kappa) \, . \tag{14}$$

Expression for C_D via measured parameters u_*, U_{max} and δ follows from equations (13-14):

$$C_D = \frac{\kappa^2}{\left(\kappa U_{\max}/u_* - \alpha\kappa + \ln(H_{10}/\delta)\right)} \, . \tag{15}$$

Wind velocity profiles were measured for 12 values of the centerline velocity from 6 m/s to 24 m/s with the resolution 0.3-0.5 cm. Each point at the velocity profile was determined by averaging over 30 sec. C_D and U_{10} were calculated by equations (15) and (11) respectively. The obtained dependency of the surface drag coefficient on 10-m wind speed is presented in fig. 4a together with the data taken from the paper by Donelan et al, 2004. The data obtained at two different facilities are rather close to each other both at the low and high wind speeds; the difference in C_D is less than 10%. The tendency to saturation of the surface drag coefficient is clearly visible for both data sets, although the thresholds of wind speeds for the saturation are slightly different (33 m/s for the data by Donelan et al, 2004 and 24.5 m/s for our data set). Possibly it is due to differences in the details of data processing.

The values of C_D obtained in laboratory by (Donelan et al., 2004) slightly exceed the data obtained in field conditions (see fig.4b). Besides, decreasing of C_D for 10-m wind speed exceeding 35 m/s reported in (Powel et al., 2003) was not observed by (Donelan et al., 2004). Our laboratory data set is in better agreement with the field data, although, extremely large wind speeds, when C_D is decreasing, were not achieved in our facility. Possibly, the differences between field and lab data are due to two main reasons. First, although similarity between lab and sea conditions[1] can be expected at strong winds, because in both cases the wave phase velocities is much less than the wind speed and then the peculiarities of the air flow over the waves are similar, the fetches in the laboratory facilities are much lower than in the field conditions. Then the waves in the lab are shorter and steeper than in the sea and enhanced aerodynamic resistance of the water surface can be expected. Second

---

[1] The question about similarity between labortory modeling of air-sea interaction and field conditions is not obvious. We will briefly discuss it in section 5.5.

reason was suggested by (Donelan et al., 2004). In laboratory facility we investigate wind-wave interaction in stationary conditions of spatially developing turbulent boundary layer. In the field conditions, the wind in hurricane eye walls is strongly unsteady and inhomogeneous flow.
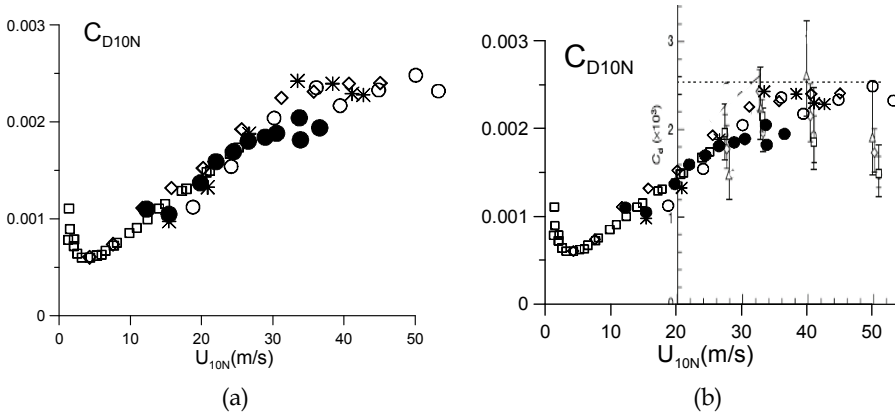

Fig. 4. Surface drag coefficient. (a) – laboratory data, black open symbols (squares, circles, diamonds, asterics) are taken from Donelan et al, 2004, closed circles – measurements at TSWiWaT, (b) – compilation of the field and laboratory data.

4.3 Wave field at strong winds in laboratory conditions

Aerodynamic roughness of the sea surface is conditioned to waves at the water surface including strong wind conditions. According to (Powel, 2007) surface drag depends significantly on the part of the tropical cyclone, where it is measured. The sea surface drag is strongly enhanced in the left front part of the tropical cyclone in comparison with right and rare parts. The data are not sufficient for final conclusions, but it seems, that the aerodynamic drag depends on the wave field, which is significantly different in different sectors of the tropical cyclone.

The wind wave field parameters in the flume was investigated by three wire gauges positioned in corners of an equal-side triangle with 2 cm side, data sampling rate was 100 Hz Three dimensional frequency-wave-number spectra were retrieved from this data by the wavelet directional method (M.Donelan et al., 1996). The wave fields at different wind speeds are characterized by narrow wave-number spectra (fig.5a) with the peak wave-number decreasing with the wind speed. It is clearly visible from fig.5a that the shapes of the spectra tend to saturation from the 10-m wind speed U_{10} exceeding 24.5 m/s. The similar tendency occurs in the dependence of the integral parameters of the wave field on the wind speed. For example, fig.5b clearly shows, that the average slope of the peak wave $S=H_s k_p/4$ (where H_s is the significant wave height, k_p is peak wave number) saturates when $U_{10}>25$m/s (see fig.5b). It means that at the wind speed about 24.5 m/s changing of the regime of the wave field occurs. Comparing the dependencies of the dominant wave slope on the wind speed with the drag coefficient dependency also shown in fig. 5b shows that the wave field regime changing correlate with saturation of the surface drag dependence of the wind speed.

The photos of top views of the water surface elucidate a possible origin of the changing of the regime of the waves wave field at 10-m wind speeds exceeding 24.5 m/s. Starting from this threshold wave breaking is intensified, because the crests of the waves are blown away by the strong tangential wind stress. It is accompanied with sprays, drops and bubbles near the wave crests, visible at the photos. Blowing away the crests of waves which steepness exceeds a definite threshold lead to the effective smoothening of the waves and the slope of the dominant wave then does not depend on wind speed as it shows fig. 6c. Basing on the theoretical model of wind turbulent boundary layer over wavy water surface, we investigated, whether this wind smoothening of the surface is sufficient for explanation the surface drag reduction.

5. Theoretical model of aerodynamic resistance of the wavy water surface at extreme wind conditions

The first step in the theoretical interpretation of the effect of the sea surface drag reduction at strong winds is calculation of the surface form grad. This part of the total aerodynamic resistance describes influence of the roughness of the surface. We can expect, that smoothening of the water surface by very strong wind significantly reduces the form drag and possibly can explain the experimental results. Then the effect of sprays and drops will be estimated.
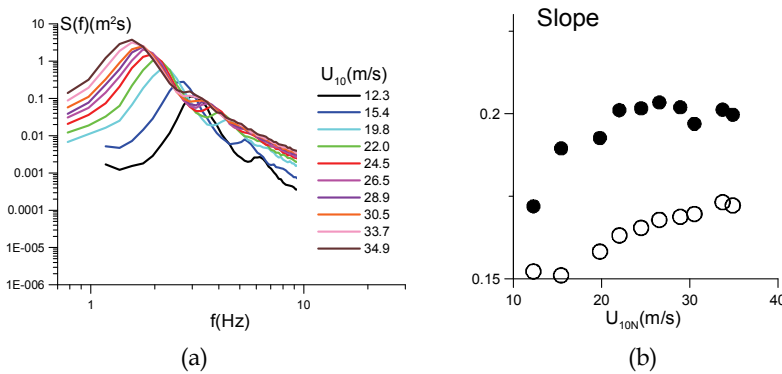

(a)   (b)

Fig. 5. Frequency power spectra of the waves for a definite fetch and different wind speeds (a) and dependence of the average slope of the peak wave (b) (open circles are the dependencies of C_D on wind speed).

5.1 The theoretical model of turbulent wind over waved water surface
The wind is regarded as a turbulent boundary layer over the wavy water surface described within the first order semi-empirical model of turbulence based on the set of the Reynolds equations:

$$\frac{\partial \langle u_i \rangle}{\partial t} + \langle u_j \rangle \frac{\partial \langle u_i \rangle}{\partial x_j} + \frac{1}{\rho_a} \frac{\partial \langle p \rangle}{\partial x_i} = \frac{\partial \sigma_{ij}}{\partial x_j}, \tag{16}$$

and the following expressions for the tensor of turbulence stresses:

$$\sigma_{ij} = \left\langle u_i' u_j' \right\rangle = \nu \left(\frac{\partial \langle u_i \rangle}{\partial x_j} + \frac{\partial \langle u_j \rangle}{\partial x_i} \right), \tag{17}$$

Here <...> denotes the quantities averaged over turbulent fluctuations, ν is the turbulent viscosity coefficient, a given function of z. We use a self-similar expression for the eddy viscosity coefficient in the turbulent boundary layer:

$$\nu = \nu_a f \left(\frac{\eta \sqrt{\tau_{turb}}}{u_*^2} \right), \tag{18}$$

where ν_a is the air molecular viscosity.

We used the approximation for f obtained by (Smolyakov, 1974) on the basis of the laboratory experiments on a turbulent boundary layer. Finally, the expression for $\nu(z)$ takes the form:

$$\nu = \nu_a \left\{ 1 + \kappa \frac{u_* \eta \sqrt{1 - \tau_{wave}/u_*^2}}{\nu_a} \left[1 - e^{-\frac{1}{L} \left(\frac{u_* \eta}{\nu_a} \right)^2 \left(1 - \frac{\tau_{wave}}{u_*^2} \right)} \right] \right\}, \tag{19}$$

In this expression L is a number, which determines the scale of the viscous sublayer of a turbulent boundary layer; it depends on the regime of the flow over the surface. Comparison with the parameters of the velocity profile in the turbulent boundary layer from (Miles, 1959) gives $L=22.4$ for hydrodynamically smooth surface, $L=13.3$ for the transition regime of a flow over surface, and $L=1.15$ for rough surface.

The boundary conditions at the air-sea interface $z=\xi(x,y,t)$ are:

$$\frac{\partial \xi}{\partial t} + \langle u \rangle \frac{\partial \xi}{\partial x} + \langle v \rangle \frac{\partial \xi}{\partial y} \bigg|_{z=\xi(x,y,t)} = \langle w \rangle \big|_{z=\xi(x,y,t)}, \tag{20}$$

$$\left\langle \vec{u}_\tau^w \right\rangle \bigg|_{z=\xi(x,y,t)} = \left\langle \vec{u}_\tau^a \right\rangle \bigg|_{z=\xi(x,y,t)}, \tag{21}$$

<u>, <v> are the x- and y- components of the velocity field in the air, averaged over turbulent fluctuations, are the tangential velocity components in water and in air.

The random field of the water surface elevation is presented as a Fourier-Stieltjes transform:

$$\zeta(\vec{r}, t) = \int dA(\vec{k}, \omega) \, e^{i(\vec{k}\vec{r} - \omega t)},$$

here $\vec{k} = \left(k_x, k_y \right)$ is a two-dimensional wave vector, ω is the frequency of surface waves.

For a statistically homogeneous and stationary process the wavenumber-frequency spectrum $F(\vec{k}, \omega)$ can be introduced as follows

$$\left\langle dA(\vec{k}, \omega) dA(\vec{k}_1, \omega_1) \right\rangle = F(\vec{k}, \omega) \delta(\vec{k} - \vec{k}_1) \delta(\omega - \omega_1) d\vec{k} d\vec{k}_1 d\omega d\omega_1,$$

To avoid strong geometric nonlinearity, the transformation to the wave-following curvilinear coordinates is performed:

$$x = \zeta_1 + \int i \, \cos\vartheta \, e^{i\left(k(\zeta_1\cos\vartheta + \zeta_2\sin\vartheta) - \omega t\right) - k\eta - i\varphi} \, dA \, ,$$

$$y = \zeta_2 + \int i \, \sin\vartheta \, e^{i\left(k(\zeta_1\cos\vartheta + \zeta_2\sin\vartheta) - \omega t\right) - i\varphi - k\eta} \, dA \, , \tag{22}$$

$$z = \eta + \int e^{i\left(k(\zeta_1\cos\vartheta + \zeta_2\sin\vartheta) - \omega t\right) - i\varphi - k\eta} \, dA \, ,$$

here φ is the angle between the wavenumber wave vector $\vec{k}$ and direction of *x*-axis. In the linear approximation, the coordinate surface η=0 coincides with the waved water surface.
The solution to the set of the Reynolds equations (16) is searched as a superposition of mean wind field $\bar{U}_0(\eta)$ and disturbances induced in the airflow by waves at the water surface. Then, the velocity field is as follows:

$$\langle\vec{u}\rangle = \vec{U}_0(\eta) + \int \vec{u}'(\eta) e^{i\left(k(\zeta_1\cos\vartheta + \zeta_2\sin\vartheta) - \omega t\right) - i\varphi - k\eta} k \, dA$$

The wave-wind interaction is considered here in the quasi-linear approximation similar to the approach developed by (Jenkins, 1992), (Janssen, 1989) and (Reutov & Troitskaya, 1995). Then the wave disturbances induced in the airflow by the waves at the water surface are described in the linear approximation and can be considered independently. The coordinate transformation (22) can be considered as a superposition of formal coordinate transformations for each single harmonic. Nonlinear terms or wave momentum fluxes enter into the equations for the components of mean velocity.
Consider first equations for the disturbances induced by a single harmonic wave at the water surface with the wave vector $\vec{k}$, frequency *ω* and amplitude *dA*. We introduce the formal coordinate transformation, where the coordinate line *η*=0 coincides with the water surface disturbed by this single harmonic wave

$$x = \zeta_1 + i\cos\vartheta \, e^{i(k(\zeta_1\cos\vartheta + \zeta_2\sin\vartheta) - \omega t) - k\eta - i\varphi} dA \, ,$$

$$y = \zeta_2 + i\sin\vartheta \, e^{i(k(\zeta_1\cos\vartheta + \zeta_2\sin\vartheta) - \omega t) - k\eta - i\varphi} dA \, , \tag{23}$$

$$z = \eta + dA e^{i(k(\zeta_1\cos\vartheta + \zeta_2\sin\vartheta) - \omega t) - i\varphi - k\eta} \, ,$$

The linear coordinate transformation

$$\zeta'_1 = \zeta_1\cos\vartheta + \zeta_2\sin\vartheta - \frac{\omega}{k}t \, ,$$

$$\zeta'_2 = \zeta_2\cos\vartheta - \zeta_1\sin\vartheta = y_2\cos\vartheta - y_1\sin\vartheta = y' \, , \tag{24}$$

defines the reference frame following this harmonic wave, where the wave field does not depend on ς_2' (or Cartesian coordinate y'), i.e. it depends only on two coordinates ς_1' and η. Tangential velocity components are transformed similar to (24), and in the new reference frame

$$u' = u\cos\vartheta + v\sin\vartheta - \frac{\omega}{k} \,,$$

$$v' = -u\sin\vartheta + v\cos\vartheta \tag{25}$$

It means that the stream function Φ can be introduced for the motions in the plane $\varsigma_2' = y' = const$ as follows

$$u' = \frac{\partial\Phi}{\partial\eta}, \ w = -\frac{\partial\Phi}{\partial\varsigma_2'} \,,$$

and the Reynolds equations can be formulated in terms of stream function Φ and vorticity χ

$$\frac{\partial\chi}{\partial t} + \frac{1}{I}\frac{\partial\chi}{\partial\varsigma_1'}\left(\frac{\partial\Phi}{\partial\eta}\right) - \frac{1}{I}\frac{\partial\chi}{\partial\eta}\left(\frac{\partial\Phi}{\partial\varsigma_1'}\right) = \Delta(\nu\chi) - \frac{2}{I^2}\nu_{\eta\eta}\frac{\partial^2\Phi}{\partial\varsigma_1'^2} -$$
$$-\frac{I_\eta}{I^3}\left((\Phi_\eta\nu_\eta)_\eta - \nu_\eta\Phi_{\varsigma_1'\varsigma_1'}\right) - \frac{I_{\varsigma_1'}}{I^3}(2\nu_\eta\Phi_{\varsigma_1'\eta} - \Phi_{\varsigma_1'}\nu_{\eta\eta}) + \Phi_\eta\nu_\eta\frac{I_{\varsigma_1'}^2 + I_\eta^2}{I^4} \,, \tag{26a}$$

$$\Delta\Phi = \chi = \frac{1}{I}\left(\Phi_{\varsigma_1'\varsigma_1'} + \Phi_{\eta\eta}\right) \tag{26b}$$

here I is the Jacobian of transformation (23). The transversal velocity component v' does not enter the equations (26a,b), and v' obeys the following equation:

$$\frac{\partial v'}{\partial t} + \frac{1}{I}\left(\frac{\partial v'}{\partial\varsigma_1'}\frac{\partial\Phi}{\partial\eta} - \frac{\partial v'}{\partial\eta}\frac{\partial\Phi}{\partial\varsigma_1'}\right) = \Delta(v'\nu) + \frac{1}{I}v_\eta'\nu_\eta \tag{27}$$

We search the solution to the system (26a,b), (27) as a superposition of the mean field and harmonic wave disturbance:

$$\Phi = \int\left(U_0(\eta)\cos\vartheta + V_0(\eta)\sin\vartheta - \frac{\omega}{k}\right)d\eta + \Phi_1(\eta)dA\,e^{ik\varsigma_1'}$$

$$v = V_0(\eta)\cos\vartheta - U_0(\eta)\sin\vartheta + V_1(\eta)dA\,e^{ik\varsigma_1'} \tag{28a}$$

$$\chi = U_{0\eta}\cos\vartheta + V_{0\eta}\sin\vartheta + X_1(\eta)dA\,e^{ik\varsigma_1'} \tag{28b}$$

Equations for complex amplitudes $\Phi_1(\eta), \chi_1(\eta), V_1(\eta)$ are obtained by linearization of system (26a,b), (27).

$$(\Phi_{0\eta}X_1 - \Phi_1\chi_{0\eta})ik - \left(\frac{d^2}{d\eta^2} - k^2\right)(X_1\nu) = -2\nu_\eta\Phi_1 k^2 - 2kAe^{-k\eta}(\Phi_{0\eta}\nu_\eta)_\eta \,, \tag{29a}$$

$$\frac{d^2\Phi_1}{d\eta^2} - k^2\Phi_1 = X_1 - 2ke^{-k\eta}\Phi_{0\eta\eta} \tag{29b}$$

$$(\Phi_{0\eta}V_1 - \Phi_1\hat{V}_\eta)ik = \nu\left(\frac{d^2}{d\eta^2} - k^2\right)V_1 + \nu_\eta V_{1\eta}k^2 \tag{30}$$

We consider solutions to the system (29a,b), (30) decreasing at large distances from the surface, i.e.

$$\Phi_1\big|_{\eta\to\infty} \to 0; \quad V_1\big|_{\eta\to\infty} \to 0$$

Boundary conditions at the water surface for the system (29a,b) follow from (20) and (21) expressed in curvilinear coordinates (see (Reutov & Troitskaya, 1995)) for details.

$$\Phi_1\big|_{\eta=0} = 0; \quad \Phi_{1\eta}\big|_{\eta=0} = 2\omega; \quad V_1\big|_{\eta\to0} = 0 \tag{31}$$

The only nonlinear effect taken into account in the quasi-linear approximation is the demodulation of the wave disturbances induced in the air flow by waves at the water surface. Equations for mean velocity profile components $U_0(\eta)$ and $V_0(\eta)$ are obtained by the following steps. Averaging of (26a,b) over ς_1' gives equation for Φ_0 and averaging of (27) yields equation for $v_0(\eta)$. Expressing $U_0(\eta)$ and $V_0(\eta)$ via $\Phi_0(\eta)$ and $v_0(\eta)$ by inversion (28a,b) and integrating over the wind wave spectrum gives:

$$\frac{d}{d\eta}\left(\nu\frac{d(U_0,V_0)}{d\eta}\right) = \int\left(\tau_\parallel(\eta,k,\varphi,\omega)(\eta)\begin{pmatrix}\cos\varphi\\\sin\varphi\end{pmatrix} + \tau_\perp(\eta,k,\varphi,\omega)(\eta)\begin{pmatrix}-\sin\varphi\\\cos\varphi\end{pmatrix}\right)k^2 F(k,\varphi,\omega)kdkd\varphi d\omega \tag{32}$$

here $\tau_\parallel(\eta,k,\theta,\omega)(\eta)$, $\tau_\perp(\eta,k,\theta,\omega)(\eta)$ are the components of the wave momentum flux induced by the surface wave with wave number k, frequency ω propagating at the angle θ to the wind.

Expression for $\tau_\parallel(\eta,k,\theta,\omega)(\eta)$ follows from (26a,b)

$$\tau_\parallel(\eta,k,\varphi,\omega)(\eta) = k\left[k\nu_\eta\,\mathrm{Re}\left(\Phi_{1\eta} - k\Phi_1\right)e^{-k\eta} + 2k^2e^{-2k\eta}\nu_\eta U_0\cos\varphi\right]$$

and expression for $\tau_\perp(\eta,k,\theta,\omega)(\eta)$ follows from (27)

$$\tau_\perp(\eta,k,\omega) = -\frac{1}{2}k\frac{d}{d\eta}\mathrm{Im}\left(\Phi_1^*V_1\right)$$

Equations (32) express the conservation law for the vertical flux of two projections of the horizontal momentum component in the turbulent boundary layer. If the turbulent shear stress at a large distance from the surface is directed along x, the conservation law for the mean momentum components may be written as follows:

$$\tau_{turb}^{(x)}(\eta) + \tau_\parallel(\eta) = u_*^2$$

$$\tau_{turb}^{(y)}(\eta) + \tau_\perp(\eta) = u_*^2$$

Since according to (32) nonlinear addition to the wind velocity profile is determined by the frequency-wavenumber spectrum $S(\omega, k, \varphi)$ of surface waves, then the spectrum is a critical component of the model. In our laboratory experiment we measured the airflow velocity profile together with the elevation of the water surface in 3 close points. These data are sufficient for retrieving 3-dimensional spectrum $S(\omega, k)$ needed for calculating the form drag and comparing with the experimental data. High frequency part of the spectrum, which can contribute to the surface roughness, was interpolated on the base of available data by the power law with the exponent determined from the experimental spectra.

5.2 Fine structure of turbulent air flow over steep and breaking waves

Let us discuss first applicability of the suggested model for description of the airflow over steep and breaking waves which occurred in the flume at strong winds. The model exploits two main suppositions: the closing hypothesis and the quasi-linear approximation for description of the the wind-wave interaction. The quasi-linear approximation presumes, that wave-induced disturbances in the air flow are considered in the linear approximation, i.e. wave-induced disturbances in the air flow are considered in the linear approximation, but the resistive effect of the wave momentum flux on the mean flow velocity profile is taken into account, i.e. within the model the mean airflow over waves is treated as non-separated.

One can expect existence of strong nonlinear phenomena such as sheltering, flow separation, etc., for the cases of steep and breaking waves. These phenomena were investigated by means of contact methods and smoke visualization in the laboratory experiments by (Banner & Melville, 1976), (Kawamura & Toba, 1979), (Kawai, 1981), (Kawai, 1982), (Hsu & Hsu, 1983), (Hsu et al., 1981). Major difficulties in these experiments are concerned with the measuring of the airflow close to the water surface, especially in the troughs of the waves. These measurements can be performed by means of the wave-following contact technique ((Hsu & Hsu, 1983), (Hsu et al., 1981), (Donelan et al., 2005). Also, the problem of measurement of the wind flow below the crests of the waves was solved by (Kawai, 1981), (Kawai, 1982) by means of seeding the flow by small particles visualized with a strobe source of light and application of special photograph technique. Kawai's experiments demonstrated occurrence of the airflow separation from the crests of steep waves on the instant images of the flow.

Recently, the structure of an airflow over waves was investigated in detail by the method of particle image velocimetry (PIV) (Adrian, 1991), when the flow is seeded with the small particles illuminated by the laser light and then taken with a digital camera. This technique was applied by (Reul et.al., 1999), (Reul et.al., 2008) and (Veron et. al., 2007) and clearly demonstrated the effect of the airflow separation from the crests of the waves and reattachment at the windward face of the wave on the instantaneous patterns of the vector velocity fields.

It should be emphasized that the PIV technique provides an instant picture of the velocity field, but the flow separation in the turbulent boundary layer over a gravity wave is a strongly non-stationary process due to both the stochastic character of the airflow and the brevity of the breaking event, which usually occurs within a small part of the wave period (Duncan et al., 1999). At the same time, the models of the air-sea fluxes and wind wave growth exploit the wind flow parameters averaged over turbulent fluctuations. We combined measurements of the instant airflow velocity fields over surface waves with

statistical averaging (Troitskaya et al., 2010). The statistical ensemble of such vector fields for subsequent averaging was obtained by means of high-speed video filming and processing of the video-films by the PIV algorithm. Individual flow realizations manifested the typical features of flow separation similar to those obtained by (Kawai, 1981), (Kawai, 1982), (Reul et.al., 1999), (Reul et.al., 2008) and (Veron et. al., 2007). The average parameters were retrieved by the phase averaging of the individual vector fields. The averaged flow patterns appear to be smooth and slightly asymmetrical, with the minimum of the horizontal velocity near the water surface shifted to the leeward side of the wave profile (compare fig.6a, b).

The results of these measurements were compared with the calculations within the quasi-linear model of turbulent boundary layer described in section 5.1. The wave parameters (wavelength, celerity, steepness), used in this comparison of theory with experiment, were retrieved from the same video films as those used for the airflow velocity calculations. The model calculations were in a good agreement with the experimentally measured and conditionally averaged mean wind velocity, turbulent stress and also amplitude and phase of the main harmonics of the wave-induced velocity components. (see fig.7a,b).
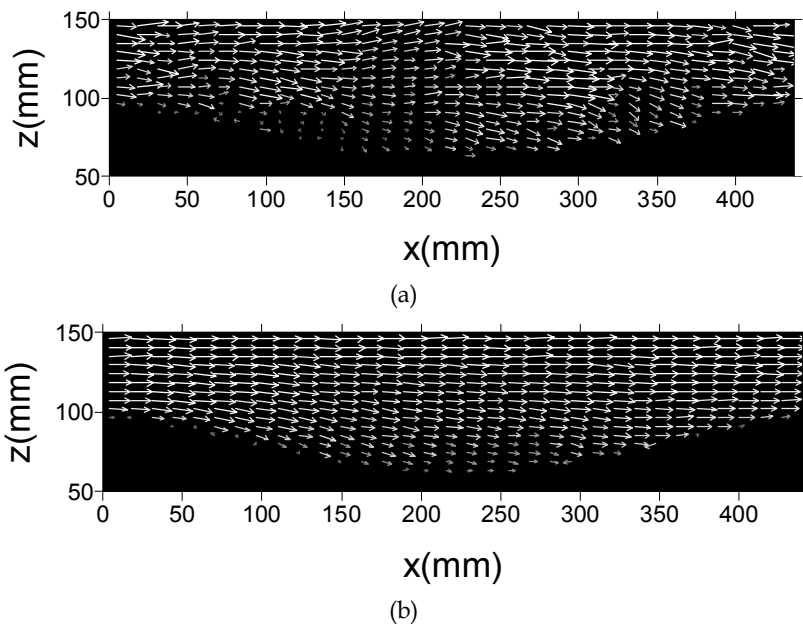

(a)

(b)

Fig. 6. The vector velocity field in the airflow over the paddle-generated wave in the wave-following reference frame retrieved from high-speed video filming by digital particle image velosimetry. Wind friction velocity u_*=200 mm/s, wavelength k=0.15 cm-1, slope ka=0.25. (a) – the instantaneous pattern, (b) ensemble averaged pattern.

Applicability of the non-separating quasi-linear theory for description of average fields in the airflow over steep and even breaking waves, when the effect of separation is manifested at the instantaneous flow images, can possibly be explained qualitatively by the strongly non-stationary character of the separation process with the typical time much less than the wave period, and by the small scale of flow heterogeneity in the area of separation. In such a situation small-scale vortices produced within the separation bubble affect the mean flow

and wind-induced disturbances as eddy viscosity. Then the turbulence of the flow affects the averaged fields as a very viscous fluid. Then the effective Reynolds number for the average fields determined by the eddy viscosity is not large even for steep waves. It follows from this assumption that strongly non-linear effects such as flow separations should be not expected in the flow averaged over turbulent fluctuations. We were encouraged by these results to apply the quasi-linear model for calculation of the form drag of the water surface at strong winds.
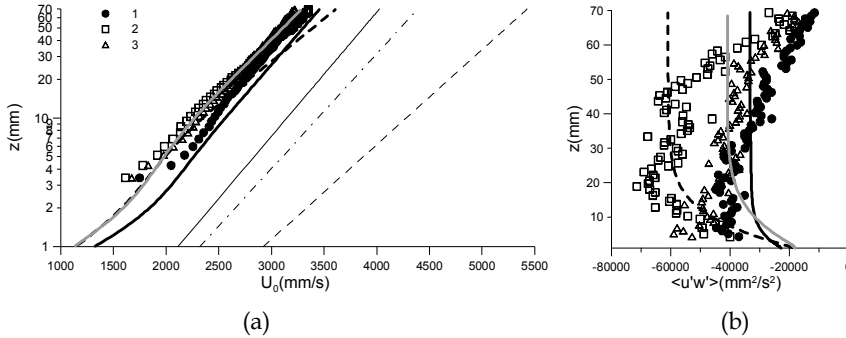

(a)   (b)

Fig. 7. Comparing theory and experiment: (a) is the mean velocity profile; (b) – the stress profile. Symbols – experiment curves – calculations within the qausi-linear model for the measured parameters of the wave and the wind (see Troitskya et al., 2010).

Dependency of the form drag of the water surface calculated within the model (29-32) for the parameters measured in the flume are presented in fig.8 together with the measured sea surface drag coefficient. It is clear that both at low and moderate winds and at strong winds (exceeding threshold value 24.5 m/s) the model is in good agreement with data. So saturation of the average slope of dominant waves enables one to explain saturation of the surface resistance, both qualitatively and quantitatively.
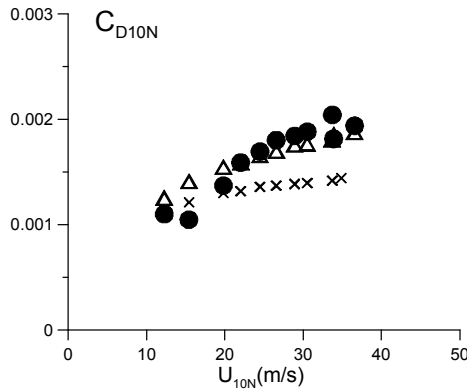

Fig. 8. Dependence of surface drag coefficient on wind speed, comparing theory and laboratory experiment. Measurements - closed circles, theoretical calculations: squares – with short wave spectrum of surface waves, crosses – neglected short wave spectrum of surface waves.

We also investigated sensitivity of the model to the spectrum of surface waves. In calculations shown in fig.8 by crosses the effect of short surface waves was eliminated by cut off surface wave spectrum at the wave number 120 m^{-1}. Comparison presented in fig.8 shows noticeable dependence of C_D on the high wave number part of the spectrum. Unfortunately, measurement of the spectrum of short waves (cm and mm wave length) with high space resolution is a difficult problem especially at strong wings. Optical methods developed by (Jähne et al, 2005), (Rosholtz, 2010) are promising for laboratory conditions.

6. Conclusion and discussion

So at extremely strong wind sea surface drag coefficient in the field and laboratory conditions demonstrates anomalous flattening or even decreasing dependency on the wind speed. Here we suggest a possible explanation of this phenomenon due to smoothening of the water surface by strong wind stress blowing away the crests of steep surface waves. This supposition is confirmed by our laboratory experiments when both wind and wave spectra were measured. Predictions of the theoretical model are in good agreement with the measurements.

It is important to discuss relation of wind-wave interaction in field and laboratory conditions at extremely strong winds. First of all, the laboratory and field conditions strongly differ in fetch. Waves in laboratory flumes are extremely "young" in comparison with nature, i.e. they correspond to the initial stage of the wave development. At this stage the phase velocity of the waves corresponding to the spectral peak c_p is small in comparison with the wind speed U_{10}. , i.e. the age parameter of the waves $c_p/U_{10}<<1$. The wind-wave interaction is the resonant process and interaction is concentrated in the layer where the wind speed is close to the phase velocity of the wave. In the theory by (Miles, 1957), (Miles, 1959) the interaction occurs in the critical layer, where the wind and wave velocities coincide. In more complicated models including the model described in section 4 the interaction occurs in a layer of constant thickness. Since the wind velocity profile is very sharp, this layer is very thin and it is positioned very close to the water surface up to $c_p<U_{10}/2$ (Phillips, 1977) and the approximation of the "young" sea is valid. Then it follows, that the region of wind-wave energy exchange is positioned close to the water surface for "young" waves and slightly depends on the wave age parameter. In other words, since "young" waves propagate much slowly than wind they interact with the wind as almost stationary surface roughness.

The wave age parameter can be easily estimated by the empirical formula suggested by (Donelan, 1985):

$$\frac{U_{10}}{c_p} = 22\left(\frac{xg}{U_{10}^2}\right)^{-1/3}$$

The wind speed distribution in a tropical cyclone is inhomogeneous. Let us first estimate the wave age parameter of waves generated by maximal wind speed, then x approximately equal to the radius of the maximum wind r_0. For a typical r_0=50 km, U_{10}=60 m/s we get U_{10}/c_p=4.3. For the gale force wind area typically x=150 km, U_{10}=20 m/s, then U_{10}/c_p=1.4. These estimates show, that the approximation of the "young sea" can be applied for description of the air-sea interaction near the radius of maximum winds similar to laboratory conditions.

Another governing parameter of the flow over rough surface is the Reynolds number, while a flow averaged over turbulent fluctuations is controlled by the effective Reynolds number Re_t determined by the effective eddy viscosity ν_t. In the case of wind-wave interaction $\nu t = u_*^2/ck$, where c and k are the phase velocity and wave number (see Troitskaya & Rubushkina, 2008). The characteristic scale of the roughness of the wavy water surface is the peak wave amplitude a_p and the airflow velocity is scaled by U_{10}. For the dominant wave the simple algebra gives

$$\mathrm{Re}_t = \frac{c_p}{U_{10}} \frac{k_p a_p}{C_D}$$

The detailed analysis of the dependency of the wave field energy on fetch (see Janssen, 2002)) gives

$$k_p a_p = 0.05 \left(\frac{c_p}{U_{10}} \right)^{-1/2}$$

and

$$\mathrm{Re}_t = \frac{0.05}{C_D} \left(\frac{c_p}{U_{10}} \right)^{1/2}$$

Taking into account that C_D at high wind is saturated at approximately 0.002 yields for the field conditions of hurricane near the region of maximal winds $\mathrm{Re}_t \approx 10$ and in the laboratory conditions $\mathrm{Re}_t \approx 5$. So, the quantities of the governing parameters in the laboratory and field conditions are close. Then we can expect, that we can model of the air-sea momentum exchange in laboratory flumes.

It should be mentioned, that there are some other effects of air-sea interaction at hurricane wind conditions, which can be specially investigated in laboratory. The hurricane wind waves are strongly affected by swell generated near the hurricane walls, where the wind speed is maximal. This swell is "mixed" with the local wind waves producing complex multi-modal spectra (Young, 2006). Effect of the swell on the sea surface drag was discussed qualitatively in (Powel, 2007). In the flumes the swell can be modelled by artificially generated long waves.

7. References

Adrian, R. J., (1991) Particle Imaging techniques for experimental fluid mechanics. *Annu. Rev. Fluid Mech.*, Vol. 23, p. 261–304.

Andreas, E. L. and K. A. Emanuel, (2001): Effects of sea spray on tropical cyclone intensity. *J. Atmos. Sci.*, Vol. 58, No 24, p. 3741-3751.

Andreas E. L. (2004) Spray stress revised. *J. Phys. Oceanogr.,* , v.34, No 6, p.1429–1440.

Barenblatt G. I. and Golitsyn G. S. (1974) Local structure of mature dust storms *J. Atmos. Sci.,* , Vol.31, No 7, p. 1917– 1933.

Donelan M.A., Haus B.K , Reul N., Plant W.J., Stiassnie M., Graber H. C., Brown O. B., Saltzman E. S. (2004) On the limiting aerodynamic roughness of the ocean in very strong winds. *Geophys. Res. Lett.*, , v.31, L18306.

Donelan M., Hamilton J. , Hui W. H. (1985) Directional spectra of wind generated waves *Philos. Trans. Roy. Soc. London, Ser. A.*, Vol 315, p.509–562.

Donelan, M. A., Babanin A. V., Young I. R., Banner M. L., McCormick C. (2005) Wave follower field measurements of the wind input spectral function. Part I: Measurements and calibrations. *J. Atmos. Oceanic Technol.*, Vol 22, No 7, No 799–813.

Donnely W. J., Carswell J. R., McIntosh R. E.   Revised ocean backscatter model at C and Ku band under high-wind conditions. (1999) *J. Geophys. Res.*, v.104, No C5, p.11485–11497.

Duncan, J. H., Qiao H., Philomin V., and Wenz A. (1999) Gentle spilling breakers: crest profile evolution. *J. Fluid Mech.*, Vol. 379, p. 191–222.

Emanuel, K.A. (1986) An air-sea interaction theory for tropical cyclones. Part I: Steady state maintenance. *J. Atmos. Sci.*, Vol. 43, No 6, p. 585-604.

Emanuel, K.A. (1995) Sensitivity of tropical cyclones to surface exchange coefficients and a revised steady-state model incorporating eye dynamics. *J. Atmos. Sci*, Vol.52, No 22, p.3969-3976.

Emanuel, K. (2003) Tropical Cyclones. *Ann Rev. Earth Planet. Sci.*, Vol. 31, p. 75-104.

Fairall C.W., Bradley E.F., Hare J.E., Grachev A.A., Edson J.B. (2003) Bulk parameterization of air–sea fluxes: updates and verification for the COARE algorithm . *J. Climate*, , Vol.16, No 4, p.571–591.

Garratt J.R. (1977) Review of drag coefficients over oceans and continents. *Mon. Weather Rev.*, , Vol.105, No7, p.915-929.

Hara T., Belcher S.E. (2004) Wind profile and drag coefficient over mature ocean surface wave spectra . *J. Phys. Oceanogr*, Vol.34, No 11, p. 2345–2358.

Hinze, J. O. (1959) Turbulence: An Introduction to its Mechanism and Theory. New York: McGraw-Hill. 586 p.

Hsu, C. T., Hsu E. Y. (1983) On the structure of turbulent flow over a progressive water wave: theory and experiment in a transformed wave-following coordinate system. Part 2. *J. Fluid Mech.*, Vol. 131, p.123–153.

Hsu, C. T., Hsu E. Y., Street R. L. (1981) On the structure of turbulent flow over a progressive water wave: theory and experiment in a transformed, wave-following co-ordinate system. *J. Fluid Mech.*, Vol. 105, p. 87–117.

Jarosz E., Mitchell D. A., Wang D.W., Teague W.J. (2007) Bottom-up determination of air-sea momentum exchange under a major tropical cyclone. *Science*, v 315, p. 1707-1709 DOI: 10.1126/science.1136466.Janssen P.A.E.M. (1989) Wave-induced stress and the drag of air flow over sea waves. *J. Phys. Oceanogr.*, , v.19, No 6, p.745-754.

Janssen P.A.E.M. (1991) Quasi-linear theory of wind wave generation applied to wave forecasting *J. Phys. Oceanogr.*, , v.21, No 11, p.1631-1642.

Jenkins A.D. (1992) Quasi-linear eddy-viscosity model for the flux of energy and momentum to wind waves using conservation-law equations in a curvilinear coordinate system. *J. Phys. Oceanogr.*, , Vol.22, No 8, p. 843–858.

Jenkins A.D. (1993) Simplified quasi-linear model for wave generation and air–sea momentum flux Journal of Physical Oceanography, Vol. 23, No 9, p. 2001–2018.

Kudryavtsev V. N. (2006) On the effect of sea drops on the atmospheric boundary layer *J. Geophys. Res.*, , Vol.111, C07020.

Jähne B., Schmidt M., Rocholz R. (2005) Combined optical slope/height measurements of short wind waves: principles and calibration Measurement Science & Technology, Vol. 16, p. 1937–1944

Kawai, S., (1981) Visualisation of air flow separation over wind wave crest under moderate wind. *Boundary Layer Meteorol*., Vol. 21, p. 93–104.

Kawai, S., (1982) Structure of air flow separation over wind wave crest. *Boundary Layer Meteorol*., Vol. 23, p. 503–521.

Kudryavtsev V., Makin V. (2007) Aerodynamic roughness of the sea surface at high winds. *Boundary-Layer Meteorol*., , v.125, p. 289–303.

Kukulka, T., T. Hara, and S. E. Belcher, (2007): A model of the air-sea momentum flux and breaking-wave distribution for strongly forced wind waves. *J. Phys. Oceanogr*., Vol 37, No 11, p. 1811-1828.

Large W.G., Pond S. (1981) Open ocean momentum flux measurements in moderate to strong winds. *J. Phys. Oceanogr.,* , Vol. 11, No 1, p.324–336.

Miles J.W. (1957) On the generation of surface waves by shear flows. *J.Fluid Mech.*,Vol.3, p.185-204.

Miles J.W. (1959) On the generation of surface waves by shear flows Part 2. *J.Fluid Mech.*, Vol.6, p.568-582.

Makin V. K. (2005) A note on drag of the sea surface at hurricane winds. *Boundary Layer Meteorol.*, , Vol. 115, No1, p.169-176.

Makin V. K., Kudryavtsev V. N., Mastenbroek C. (1995) Drag of the sea surface. *Boundary-Layer Meteorol.*, Vol.79, p.159–182.

Phillips O. M. (1977) *The Dynamics of the Upper Ocean.* Cambridge Monographs on Mechanics Cambridge University Press; 2 edition), ISBN-10: 0521298016, ISBN-13: 978-0521298018

Powell, M.D., Vickery P.J., Reinhold T.A. (2003) Reduced drag coefficient for high wind speeds in tropical cyclones. *Nature* , v.422, p.279-283.

Powell M. D. (2007) Final Report "Drag Coefficient Distribution and Wind Speed Dependence in Tropical Cyclones"Principal In vestigator: Mark D Powell NOAA/AOML, 2005-2007, Taylor P.K., Yelland M.J. (2001) The dependence of sea surface roughness on the height and steepness of the waves. *J. Phys. Oceanogr.*, , v.31, No 2, p.572–590.

Reul, N., Branger H., Giovanangeli G.P. (1999) Air flow separation over unsteady breaking waves. *Phys. Fluids*, , v.11, No 7, p.1959-1961.

Reutov, V.P. and Yu. I. Troitskaya, (1995) On the nonlinear effects in the interaction of gravity waves with turbulent airflow. *Izvestiya, Atmospheric and Oceanic Physics*, Vol. 31, No 6, p. 825–834.

Rocholz R., Jähne B. (2010) Spatio-temporal measurements of short wind water waves EGU General Assembly, Symposium AS2.2, EGU2010-5509,

Smolyakov, A. V., (1973) Spectrum of the quadruple radiation of the plane turbulent boundary layer. Acoust. Phys., Vol 19, No 3, p. 420–425

Yu. I. Troitskaya, G. V. Rybushkina. (2008) Quasi-linear model of interaction of surface waves with strong and hurricane winds. *Izvestiya, Atmospheric and Oceanic Physics* Vol. 44, No 5, p. 621-645

Tsimplis, M. , Thorpe S. A. (1975): Wave damping by rain. *Nature*, Vol.342, p. 893-895.

Veron F., Saxena G., Misra S. K., (2007) Measurements of the viscous tangential stress in the airflow above wind waves. *Geophys. Res. Lett.*, Vol. 34, L19603, doi: 10.1029/2007GL031242.

R. Young (2006) Directional spectra of hurricane wind waves *J. Geophys. Res*, Vol. 111, C08020, doi: 10.1029/2006JC003540,